NANO LETTERS

Letter

pubs.acs.org/NanoLett

The Role of External Defects in Chemical Sensing of Graphene Field-Effect Transistors

B. Kumar,[†] K. Min,[‡] M. Bashirzadeh,[§] A. Barati Farimani,[‡] M.-H. Bae,[∥,⊥] D. Estrada,[∥] Y. D. Kim,[#] P. Yasaei,[†] Y. D. Park,[#] E. Pop,[∥] N. R. Aluru,[‡] and A. Salehi-Khojin*,[†]

[†]Department of Mechanical and Industrial Engineering, University of Illinois at Chicago, Chicago, Illinois 60607, United States

[‡]Department of Mechanical Science and Engineering, Beckman Institute for Advanced Science and Technology, University of Illinois at Urbana−Champaign, Urbana, Illinois 61801, United States

[§]Department of Mechanical Engineering, North Dakota State University, Fargo, North Dakota 58102, United States

[∥]Department of Electrical and Computer Engineering, Micro and Nanotechnology Laboratory, University of Illinois at Urbana−Champaign, Urbana, Illinois 61801, United States

[⊥]Korea Research Institute of Standards and Science, Daejeon 305-340, Republic of Korea

[#]Department of Physics and Astronomy, Seoul National University, Seoul 151-747, Republic of Korea

Supporting Information

ABSTRACT: A fundamental understanding of chemical sensing mechanisms in graphene-based chemical field-effect transistors (chemFETs) is essential for the development of next generation chemical sensors. Here we explore the hidden sensing modalities responsible for tailoring the gas detection ability of pristine graphene sensors by exposing graphene chemFETs to electron donor and acceptor trace gas vapors. We uncover that the sensitivity (in terms of modulation in electrical conductivity) of pristine graphene chemFETs is not necessarily intrinsic to graphene, but rather it is facilitated by external defects in the insulating substrate, which can modulate the electronic properties of graphene. We disclose a mixing effect caused by partial overlap of the highest occupied molecular orbital (HOMO) and lowest unoccupied molecular orbital (LUMO) of adsorbed gas molecules to explain graphene's ability to detect adsorbed molecules. Our results open a new design space, suggesting that control of external defects in supporting substrates can lead to tunable graphene chemical sensors, which could be developed without compromising the intrinsic electrical and structural properties of graphene.

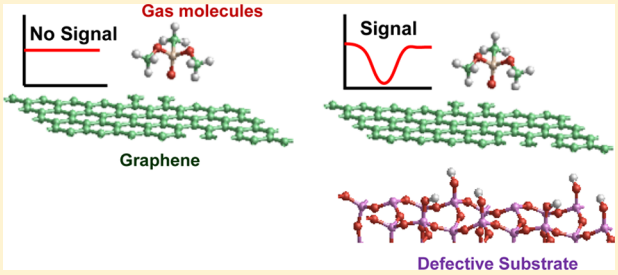

KEYWORDS: *Graphene, chemFETs, chemical sensors, defects, density functional theory (DFT)*

As we are near the 10th anniversary of its discovery,[1] it is evident that graphene has been one of the most studied materials of the past decade due to its exceptional electrical,[2] mechanical,[3] and thermal properties.[4,5] Despite a short history, it has attracted huge scientific interest and as a result has been used in numerous advanced technological fields such as photonics,[6] high-frequency electronics,[7] nanoelectromechanical systems for mass detection,[8] nanopores for DNA[9] and DNA−protein complex detection,[10] and highly sensitive gas sensor[11] devices. In particular, the high specific surface area (~2600 m^2/g) of graphene offers each atom as an adsorption site for an analyte molecule. Moreover, the high carrier mobility of graphene (~2500 to 40 000 $cm^2 V^{-1}s^{-1}$ for supported graphene depending on temperature, carrier density, and substrate phonons)[12,13] and low $1/f$ noise compared to other solid state sensors[14] makes it an exceptional candidate for chemical or biomarker sensing applications as highlighted in recent reviews.[15,16] Previous studies have reported that graphene sensors can be integrated by using graphene produced via different routes, for example by mechanical exfoliation,[17,18] chemical vapor deposition (CVD),[19] chemical exfoliation,[20,21] or sublimation of Si from SiC substrates.[22] However, different synthesis and fabrication processes result in graphene with different atomic structures; i.e., pristine and monocrystalline, as well as defective and polycrystalline. In the latter case, defects can be in the form of grain boundaries, ripples, wrinkles, and point defects, resulting in sp^3-like character at defects sites within the graphene crystal structure.[23,24]

While our groups[19,20,25,26] and others[14,17,21,27] have extensively studied the sensing mechanisms in defective graphene and carbon nanotubes (CNTs), at this point, the operational mode of pristine graphene sensors is not as well-understood as in defective carbon nanomaterial based detectors.[27] For instance, we have recently shown that sp^3-like character of defect sites in graphene and CNT sensors can form low-energy

Received: December 22, 2012
Revised: April 15, 2013
Published: April 15, 2013

sorption sites for analyte molecules.[19,25] This results in an inherent potential to significantly influence the electrical response of carbon-based sensors for a broad spectrum of chemical vapors. It has been shown that the Poole−Frenkel conduction regime, where an electron "jumps" through these defects, is key to enhancing the sensitivity and reversibility of these sensors.[25]

In this study, we aim to explore the governing mechanisms of gas detection in pristine graphene-based chemical field-effect transistors (chemFETs). We focus on the idea that the operational mode of defect-free graphene should be completely different from defective graphene obtained by CVD or chemical exfoliation. The question we then ask is "How does the structure of pristine graphene interact with adsorbed molecules if there are no low energy sorption sites on its surface resulting from defects?" In particular, we aim to discover: (i) if the adsorption of molecules on the graphene surface results in charge transfer between the two, or if the measured response is due to Coulomb scattering, and (ii) how and if shifting the Fermi level contributes to the sensitivity and reversibility of the sensor. In contrast to graphene nanoribbon sensors,[28] we focus on large-scale graphene sheets where edges and low densities of point defects are not expected to play a significant role in chemical sensing.[19,29] To this end, we used gas sensing experiments and performed systematic density functional theory (DFT) simulations to understand the details of the interactions between gas molecules and a pristine graphene chemFET device.

Experimentally, a pristine monocrystalline graphene sheet was obtained by micromechanical cleavage of graphite and transferred onto an n-doped Si substrate with a thin SiO_2 insulating layer (t_{ox} = 100 nm). The chemFET was fabricated using standard electron beam-lithography for electrode deposition and graphene channel definition. The detailed device fabrication procedure has been published elsewhere.[19] Figure 1a and b shows the schematic representation of our fabricated device under sensing conditions and the corresponding scanning electron microscopy (SEM) image, respectively. In addition, Raman spectroscopy (Renishaw confocal microscope with 633 nm excitation laser and spot size ~1 μm) was used to evaluate the quality and number of graphene layers. We took point Raman spectra at various positions along the graphene sheet after device fabrication and found the absence of a D-band (at ~1350 cm^{-1}) indicative of high quality graphene (Figure 1c). We note the absence of the D-band does not necessarily guarantee the sample is defect-free, only that the density for Raman-active defects is below the detection limit of the instrument.[30] Previous studies of mechanically exfoliated graphene, however, indicate such samples typically have a very low density of point defects,[31] which are not expected to play a significant role in electrical transport or chemical sensing unless their density is high enough to induce a D-band in the Raman spectra.[29,32] The low full width at half-maximum (fwhm) value of the 2D-band (~31 cm^{-1}) and high I_{2D}/I_G ratio (~3.8) indicates the graphene is monolayer.[33] Prior to investigating the sensing characteristics, we examine the electrical properties of the graphene device. The scattered dots in Figure 1d show the measured graphene resistance with respect to applied gate-to-drain voltage (V_{gd}) at low source-to-drain bias, V_{sd} = 20 mV. The resistance approaches the charge neutrality point (point of the highest resistance) near $V_{gd} \approx V_{Dirac} \approx 28$ V, indicating the p-type nature of the graphene device. The p-type behavior of our graphene chemFET is attributed to the charge transfer from ambient oxygen and water molecules existing between the graphene and the substrate and the doping from the underlying SiO_2.[34]

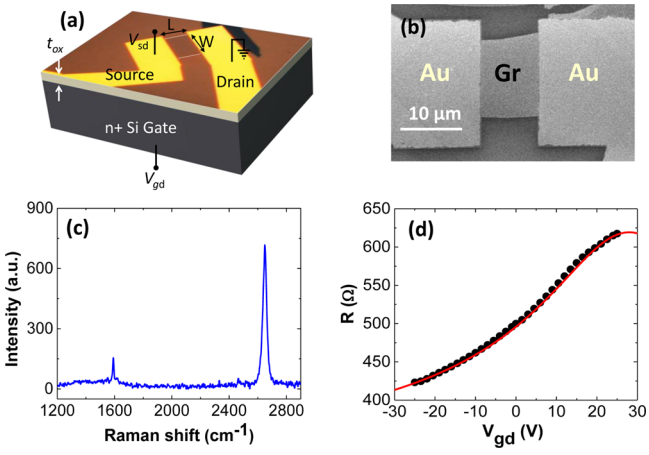

Figure 1. Characteristics of graphene device. (a) Schematic diagram of graphene device with source, drain, and n-doped Si gate. (b) Scanning electron image of the graphene channel (Gr) and contacts (Au). (c) Raman point spectra of mechanically exfoliated graphene following device fabrication confirming high quality monolayer graphene and (d) resistance of graphene device with respect to gate voltage (scattered points: experiment, solid curve: fit-result).

Next, the sensors were exposed to known concentrations of dimethyl methylphosphonate (DMMP) and to 1,2-dichlorobenzene (DCB) gas molecules, while the change in the source-to-drain current (I_{sd}) of the device was measured at different V_{gd} and V_{sd} conditions. Figure 2a and b shows the sensing response of our graphene chemFET when exposed to DCB and DMMP molecules, respectively. The V_{sd} was kept constant (100 mV), and the chemo-electrical signals were recorded at different applied V_{gd} (−20 to 20 V) while the graphene chemFET was exposed to a 100 ms pulse of trace gas vapors. The pulse conditions provide ~10^{15} molecules of DCB (electron acceptor) or ~10^{13} molecules of DMMP (an electron donor). Varying the V_{gd} allows us to investigate the effect of gate-induced carrier modulation within the graphene channel on the chemFET sensing performance. The sensitivity has been measured by calculating the ratio of percent change in current and initial current, i.e., $\Delta I_{sd}/I_{sd0}$. Clearly, the DCB and DMMP molecules show sharp signals and completely contrasting sensing patterns to each other. These results indicate that the response we observed here is not due to simple Coulomb scattering of charge carriers with the adsorbed gas molecules. In this scenario we could expect a reduced conductivity of the sensor upon exposure to both electron donor and electron acceptor gas molecules, which is not the case here. To understand the role of the metal contacts we extracted the contact resistance (R_c) (resistance between the Ti/Pd electrode and the graphene sheet) by fitting the low-bias $R-V_{gd}$ characteristics (details are in the Supporting Information). From our best fit we estimate the R_c of our device is 28 Ω near the charge neutrality point (V_{Dirac}) (Figure 2c). The extracted resistance of the graphene device, R is shown in Figure 1d (solid line), where the carrier mobility is 2500 $cm^2\ V^{-1}\ s^{-1}$, the charge neutral point is ~28 V, and the impurity density is n_0 = 2.18×10^{12} cm^{-2}.[35] Varying the carrier mobility in our model (500−3000 $cm^2\ V^{-1}\ s^{-1}$) gives a total range for R_c from 18−40 Ω across V_{gd} = −25 to 25 V, respectively. Within this range, R_c

dx.doi.org/10.1021/nl304734g | Nano Lett. 2013, 13, 1962−1968

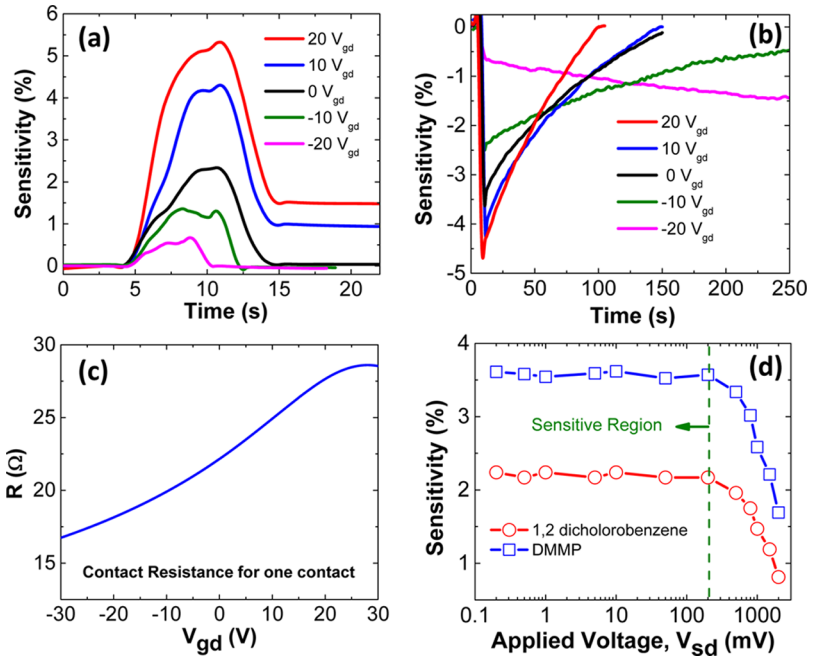

Figure 2. Sensing performance of graphene device to gas molecules: (a) 1,2-dichlorobenzene (DCB) shows a positive response which increases with applied V_{gd} while (b) dimethyl methylphosphonate (DMMP) molecules exhibit a negative response with a similar increase in the magnitude of sensitivity with respect to applied V_{gd}. The sensitivity has been measured by calculating the ratio of change in current to initial current $\Delta I_{sd}/I_0$ in percentage. (c) Calculated contact resistance from the fit in Figure 1d. The low magnitude of the contact resistance confirms that the resistance change due to the chemical gas originates mainly from the graphene channel. (d) Variation in the maximum sensitivity with respect to applied V_{sd} from 0.1 to 1000 mV at V_{gd} = 0 V. The sensitivity is independent of change in V_{sd} up to 200 mV and then decreases with increasing V_{sd}.

accounts for a maximum of ∼14% of the total device resistance at low hole densities (V_{gd} = 25 V). This indicates R_c has a negligible influence on the response of our sensors.[36]

It must be noted that DCB is an electron acceptor while DMMP is an electron donor molecule. Therefore, once the vapor molecules come into contact with graphene, the adsorbed molecule is expected to change the charge carrier distribution instantaneously. In the case of exposure to DCB molecules we expect the DCB to accept an electron from the graphene device and enhance the hole charge carrier density, leading to an improvement in overall conductivity, as we are operating the sensor in the hole-doped regime. Thus we observe a sharp response (high sensing curve slope) immediately, and further the sharpness decreases gradually with time. In contrast, DMMP molecules donate electrons to graphene which neutralizes the hole charge carriers and thus partially diminish the total charge carrier density. The reduction in charge carrier density results in a drop in current and thus negative sensing signals.

In addition to sensing performance, Figure 2a and b also illustrates the effect of V_{gd}, i.e., the effect of variation in charge carrier density on sensitivity. By varying the V_{gd} from −20 to 20 V, the device operational point of the sensor with respect to charge carrier density shifts toward the charge neutrality point. Near the charge neutrality point the chemFET is exceptionally sensitive to variations in the number of charge carriers. For instance, as we increase the V_{gd} from −20 to 20 V, we observe that the sensitivity of the device operated at V_{gd} = 20 V is approximately 10 times higher than the sensitivity at V_{gd} = −20 V. Additionally, varying the V_{gd} permits us to probe the recovery time of the device under ambient conditions, which is a measure of the adsorption strength of gas molecules to the graphene surface. Interestingly, we find that the recovery time is significantly different for DCB and DMMP. When the chemFET is exposed to DCB, we find the recovery time gradually increases when we sweep the V_{gd} from −20 to 20 V. In the case of DMMP, recovery time decreases. The different recovery time and distinct phenomena with the applied gate potential can be understood in terms of gas molecule desorption energy barriers similar to CNT devices.[26]

Next, we kept the back-gate voltage at V_{gd} = 0 and changed V_{sd} over the wide range between 0.2 and 1000 mV (Figure 2d). The sensitivity of the device to DCB and DMMP is consistent up to V_{sd} = 200 mV indicating that within this range there is no effect of the applied V_{sd} on the absorption/desorption of trace gas vapor molecules. We observed, however, that beyond V_{sd} = 200 mV, the sensitivity decreases radically. We realized that the trend observed in V_{sd} range of 0.2−200 mV for pristine graphene is different from that of defective graphene and CNT sensors. In our previous work, we have shown that defective graphene and CNT sensors are insensitive to gas adsorption at low applied voltages until a critical potential is reached.[19] The sensor response then rapidly increases over a small range of voltage. The critical voltage roughly corresponds to the barrier for electron hopping between defect sites. However, for pristine graphene chemFETs, we did not observe a critical potential for the device sensitivity, suggesting that the sensing mechanism of pristine graphene is different from defective graphene and CNTs.

To gain an in-depth understanding of the operational mode of pristine graphene sensors, we performed systematic DFT calculations. We investigated the role of pristine graphene and the supporting substrate independently, prior to combining the two into the materials system which mimics actual experimental conditions. We also studied the molecular bond structure of DCB and DMMP in terms of bond lengths and bond angles at

dx.doi.org/10.1021/nl304734g | Nano Lett. 2013, 13, 1962−1968

their fully relaxed stage (the maximum residual force < 0.01 eV/Å), and values are in good agreement with previous work (Supporting Information, Figure S1).[37,38] We note that DCB or DMMP molecules can be adsorbed by various means on the graphene surface; therefore, four different configurations were considered, configurations A–D (Figure S2). The initial gap between gas molecules and graphene was 3 Å for DCB and 2.8 Å for DMMP under the assumption that direct chemical bonding does not exist between the adsorbed molecules and the graphene. The binding energy was calculated by subtracting the energy of the adsorbed gas molecules and graphene from the total energy of the system. The lowest binding energy (E_b) has been perceived for configuration position C (DCB-graphene) and B (DMMP-graphene), respectively (Table S1). We note that there is no significant difference of binding energy among different configurations, suggesting that the interaction between graphene and the gas molecule is independent of the molecule configuration on the graphene layer.

In our simulations, we first considered gas molecules deposited on pristine graphene (free-standing) with and without water molecules. Each structure is fully relaxed, and then the local density of states (LDOS) for graphene is extracted. We observed that both DCB and DMMP gas molecules do not disturb the LDOS of graphene significantly, particularly near the charge neutrality point (Figure 3a). This suggests the gas molecules are physically adsorbed (physi-orption) on the graphene surface. In this non-bonding configuration, the adsorbed gas molecules are in contact with graphene by means of weak van der Waals forces.[39] These forces do not create a significant deviation in the graphene lattice; hence, the fundamental electronic features of graphene are not altered. We performed additional simulations using two DMMP molecules to confirm the negligible effect of gas molecules on the graphene LDOS, which is not due to the lack of number of gas molecules (Figure S3), and again, no difference is observed in the LDOS spectrum of graphene. This confirms that the inconsequential effect is independent of the number of adsorbed gas molecules.

Next, we investigated pristine graphene on pristine SiO_2, i.e., defect-free graphene supported by an idealized (e.g., absence of Si and/or oxygen dangling bonds), charge neutral substrate which is unlike that in our experiments but readily achieved in simulations. The LDOS of pristine graphene on defect-free SiO_2 overlaps with the LDOS of freely suspended pristine graphene (Figure 3b). This suggests that the electronic properties of pristine graphene are not altered when graphene is directly placed on pristine SiO_2. It should be noted that both pristine graphene and pristine SiO_2 are highly inert materials. The deposition of pristine graphene over pristine SiO_2 indicates that two inert materials are put together and consequently, charge transfer does not take place between the idealized substrate and graphene. As a result no doping of the graphene occurs, resulting in no shift of the Dirac point of graphene. With the defect-free SiO_2, water molecules are also integrated in the system by considering that water molecules exist at the interface between graphene and the pristine SiO_2 substrate. The LDOS spectrum of the system perfectly coincides with the pristine graphene LDOS spectra. Therefore, we conclude water molecules have an insignificant impact on the LDOS of graphene. In addition, the presence of water molecules does not have a substantial impact on the LDOS of graphene even with adsorption of DCB or DMMP molecules (Figure 3c). Thus, on the basis of the above result we can conclude that neither the idealized SiO_2 substrate nor the water molecules are solely responsible for the electronic sensing performance of graphene-based chemFET sensors.

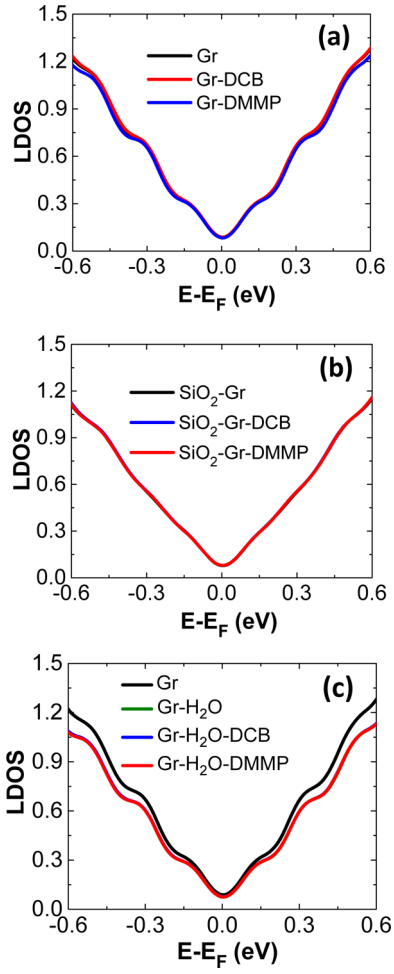

Figure 3. Local density of states (LDOS) of graphene (Gr) device calculated by DFT: (a) The LDOS spectrum of pristine and suspended graphene is not influenced by the absorption of DCB or DMMP gas molecules and (b) if pristine graphene is placed on defect-free SiO_2 the LDOS of the device remains unperturbed. Moreover (c) pristine graphene placed on defect-free SiO_2 and in the presence of water molecules underneath the graphene does not exhibit an induced doping effect. As a consequence the Dirac point position remains constant. Some curves are not visible because they overlap with others.

Next, we simulated a more realistic materials system similar to that used in experiments, i.e., defective SiO_2 with pristine graphene and different numbers of water molecules. To mimic the experimental condition, cristobalite type SiO_2 which induces p-type characteristics to graphene is constructed for the simulations.[40] An alternative scenario is to use amorphous SiO_2 in the presence of O_2 and N_2 molecules.[41] It is worth noting that in the latter case, the only role of O_2 and N_2 is to modulate the electronic structure of the graphene, and they are expected not to participate in the sensing process (interaction with DMMP and DCB molecules). Thus, in either of these simulations, the sensing mechanism of the graphene is the same as long as the electronic structure of the graphene remains the same.

In the first set of simulations, there are no water molecules, and thus graphene interacts directly with defective SiO_2. It is clearly shown in Figure 4a that the Dirac point is shifted from

dx.doi.org/10.1021/nl304734g | Nano Lett. 2013, 13, 1962–1968

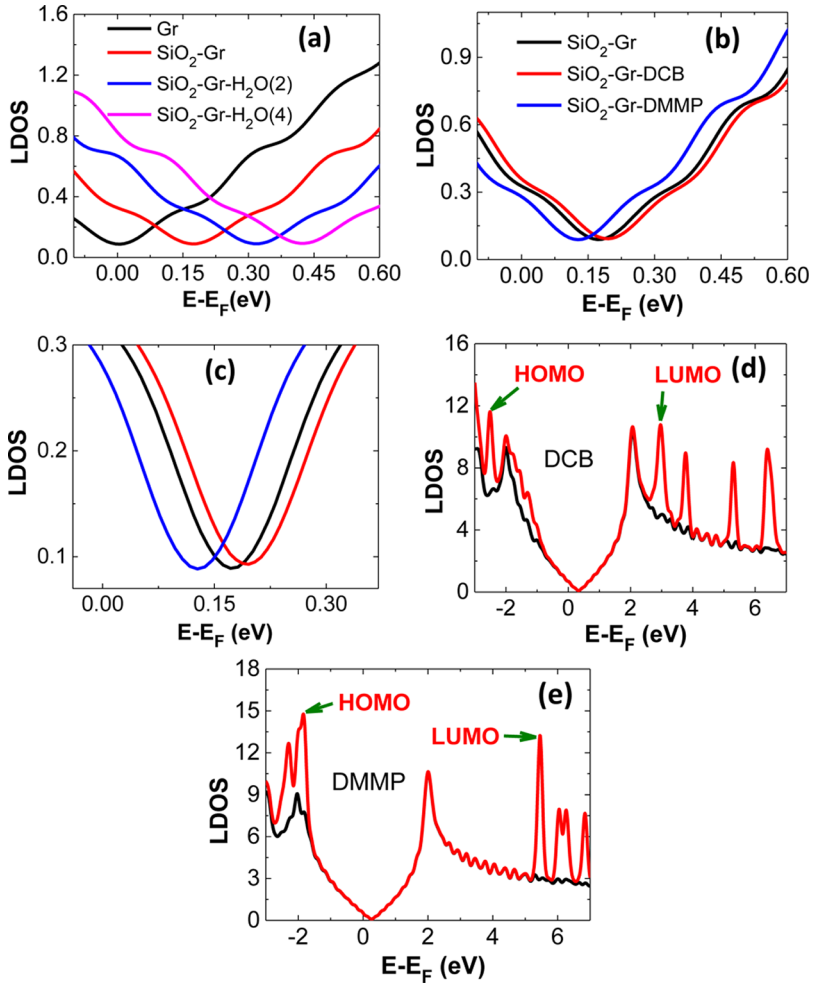

Figure 4. LDOS of (a) suspended graphene (Gr) and graphene on defective SiO_2 alone or in presence of water molecules considered between graphene and defective SiO_2, and (b) LDOS of graphene on defective SiO_2 after DCB and DMMP molecule adsorption, (c) the zoom-in of the LDOS at the Dirac point from (b) to visualize the gap between the LDOS of graphene and DCB and DMMP. (d and e) LDOS of graphene (on defective SiO_2) in black and highest occupied molecular orbital (HOMO) and lowest unoccupied molecular orbital (LUMO) spectra of DCB and DMMP molecule (in red), respectively.

zero toward higher energies. The shift in Dirac point is approximately 0.18 eV, and the charge transfer based on Mulliken charge population is 0.362*e*, where *e* is the elementary charge. In the case of defective SiO_2, defect induced dangling bond states for the Si substrate atoms create electron efficiency sites into the substrate. This gives rise to the charge transfer process between graphene and SiO_2, which slightly distorts the graphene planar lattice and p-dopes the graphene.

Figure 4a also illustrates the effect of the density of water molecules placed between graphene and defective SiO_2 on the LDOS. We found that the presence of water molecules can enhance the doping level of the graphene film if they are placed on defective SiO_2, while no effect on the LDOS is observed if the substrate is pristine (Figure 3c). It should be considered that water molecules are very sensitive to external electrical fields and thus can be polarized at the defective SiO_2 surface generating a net negative charge which further generates equal positive charge on the graphene layers.[42,43] As shown in Figure 4a, increasing number of water molecules can further shift the LDOS of graphene to higher energies (~100 meV when increasing from 2 to 4 water molecules).[42] In addition, the charge transfer is 0.184*e* and 0.328*e* for 2 water and 4 water molecules, respectively.

Figure 4b and c illustrates the effect of adsorbed gas molecules on graphene deposited over defective SiO_2. We observed that the LDOS of the system is shifted to the right (~0.02 eV) and left (~0.05 eV) due to adsorption of DCB and DMMP molecules, respectively. Charge transfer also supports the result that DCB acts as an electron acceptor and DMMP an electron donor; thus as a result, in the presence of DCB and DMMP molecules the LDOS of graphene is shifted to lower and higher energies, accordingly. In terms of the change in the position of the Dirac point, DCB molecules are less effective than DMMP, which is consistent with our experimental results.

To understand the charge transfer mechanisms, understanding the relative states of the highest occupied molecular orbital (HOMO) and the lowest unoccupied molecular orbital (LUMO) of graphene and gas molecules is of fundamental importance. In relation to the relative position of the HOMO and the LUMO, three states can be found: (i) the HOMO where the valence band is maximum, (ii) the LUMO where the conduction band is minimum, and (iii) the Fermi level of graphene. For the first and second scenarios, the charge transfer will occur from the molecule to graphene and graphene to the molecule, respectively. In the last case, the charge transfer between graphene and gas molecules can be determined by the

dx.doi.org/10.1021/nl304734g | *Nano Lett.* 2013, 13, 1962−1968

overlapping or mixing of the HOMO or LUMO with the graphene orbital hybridization.[39,44] Figure 4d and e elucidates the orbital structure of graphene and graphene with DCB and DMMP molecules. For the DCB case, the HOMO and LUMO are equally close to the Dirac point. However, a close examination reveals that the position of the HOMO (−2.83 eV) and the LUMO (2.65 eV) is different considering the Dirac point of graphene is at 0.31 eV. Thus the LUMO (DCB) is closer to the graphene Dirac point, and hence charge transfer occurs from graphene to DCB. In the case of DMMP, the HOMO (−1.85 eV) of DMMP largely overlaps with the graphene Fermi level, and the LUMO (5.16 eV) is far from the Dirac point of graphene. As a result DMMP works as an electron donor. This explains the larger charge in DMMP (∼0.05e) compared to DCB (∼0.02e). On the basis of these observations, we propose a new sensing concept that a mixing effect caused by partial overlap of the HOMO and LUMO of adsorbed gas molecules on graphene is mainly responsible for the sensing performance of graphene chemFETs.

Finally, Figure 5 shows the effect of DMMP molecules on the structure of defective SiO_2-graphene with varying numbers

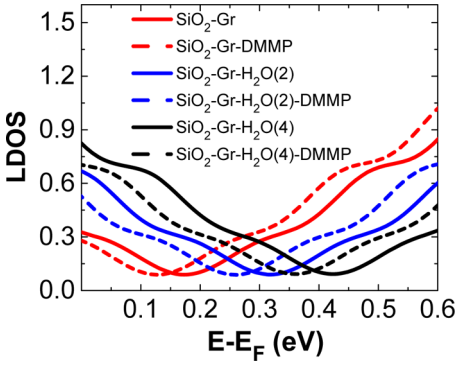

Figure 5. LDOS for graphene placed on defective SiO_2 with water (2 and 4) and DMMP (2 and 4) molecules. Dirac point shift to positive region with adsorption water molecules (solid lines) and in contrary shifts to the left in the presence of DMMP molecules (dashed lines).

of water molecules. After the adsorption of DMMP molecules, the Dirac point is shifted to the left by approximately 0.05 eV in the absence of water. When water is present, the Dirac points are shifted to the left by 0.053 and 0.057 eV for two and four water molecules cases, respectively. The charge transfer information for each system is summarized in Table 1, and it

Table 1. Charge Transfer for Gas Molecules in the Case of Pristine Graphene Placed on Defective SiO_2 without Considering Water Molecules and with Water Molecules[a]

	DCB	DMMP
no water	0.026e	−0.05e
2 water	0.024e	−0.048e
4 water	n/a	−0.055e

[a]Negative sign means the gas molecule gives this charge to graphene.

shows that the effect of water molecules on the charge transfer of DMMP is not significant. These results suggest that, in the presence of gas molecules, water molecules work like a charge carrier media as they enhance the conductivity and doping level of the system but do not promote the charge transfer process from the gas molecule to graphene.

To verify the DFT results, further sensing experiments were performed on suspended graphene devices (Figure 6a). The

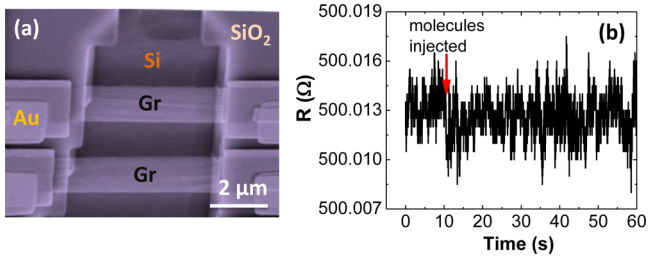

Figure 6. (a) SEM image of suspended graphene channels (indicated by Gr) and contacts (Au). In the contact regions, the graphenes are sandwiched between two slightly mismatched gold electrodes (see the fabrication details in the SI file). The depth of the trench is 1 μm. (b) The resistance vs time plot of suspended graphene based sensors shows no significant response to ∼10^{15} DCB molecules. The sensing experiments were done at V_{sd} = 0.1 V.

details of the fabrication procedure are described in the Supporting Information. We injected a wide range of number of gas molecules (∼10^{13}−10^{17} molecules of DCB and DMMP) and did not observe any response (the ratio of change in current and initial current in percentage) from the suspended devices. The initial resistance ∼500 Ω remained constant. Figure 6b shows the obtained raw data (the change in resistance with respect to time). We also fabricated pristine graphene resistors on hydrogen-passivated SiO_2 substrates (300 nm SiO_2 on Si, see the Supporting Information). It should be noted that hydrogen atoms at elevated temperature, e.g. 400 °C, saturate the dangling bonds in SiO_2 and thus reduce the density of defects (e.g., dangling bonds) significantly.[45,46] Interestingly, pristine graphene sensors fabricated on hydrogen-passivated SiO_2 also did not display a noticeable response when exposed to a similar number of gas molecules (Figure S5B in Supporting Information). Thus, these experimental results further confirm that external defects (in substrate) dominate the sensing characteristics of pristine graphene-based chemFETs or chemresistors. The obtained results strongly support the DFT conclusions as discussed above.

In conclusion, our experimental results suggest the sensing mechanism of pristine graphene chemFETs is not similar to that of defective graphene chemFETs where defects in the graphene lattice are dominant factors controlling the sensing characteristics of the device. Second, our study elucidates that pristine graphene-based chemFETs are not strongly intrinsically sensitive (in terms of modulation of electrical conductivity) to adsorbed gas molecules. Instead, we found that defective substrates are needed to more strongly modulate the electrical properties of graphene. In this respect, external defects are shown to be responsible for the sensing characteristics of pristine graphene chemFETs. Finally, based on theoretical analysis, we explored that the sensing mechanism for graphene chemFETs is based on partial overlap of the HOMO and LUMO of adsorbed gas molecules and graphene on defective SiO_2. This suggests graphene chemFET sensitivity could be tailored by engineering the substrate properties. Therefore, these results will be highly beneficial for designing and engineering graphene chemFETs for various applications such as sensors and electronic devices.

dx.doi.org/10.1021/nl304734g | Nano Lett. 2013, 13, 1962−1968

■ ASSOCIATED CONTENT

Supporting Information

Supplementary figures and detailed descriptions of DFT calculations. This material is available free of charge via the Internet at http://pubs.acs.org.

■ AUTHOR INFORMATION

Corresponding Author

*E-mail: salehikh@uic.edu.

Author Contributions

B.K. and K.M. contributed equally to this work. M.B., A.B.F., and M.-H.B. contributed equally to this work.

Notes

The authors declare no competing financial interest.

■ ACKNOWLEDGMENTS

This work was in part supported by University of Illinois at Chicago. The work at the University of Illinois Urbana−Champaign was supported in part by the Office of Naval Research (M.-H.B. and E.P.) and the National Defense Science and Engineering Graduate (NDSEG) Fellowship (D.E.). NRA research was supported by the National Science Foundation under grants 0941497 and 1127480. Y.D.K. and Y.D.P. were supported by the National Research Foundation of Korea (NRF) grant funded by the Korea government (MEST) (No. 2012-014248, 2012-0006233, 2012-0000606). We also thank H. S. Kim and S. W. Lee for suspended graphene fabrication assistance.

■ REFERENCES

(1) Novoselov, K. S.; Geim, A. K.; Morozov, S. V.; Jiang, D.; Zhang, Y.; Dubonos, S. V.; Grigorieva, I. V. *Science* **2004**, *306*, 666−669.

(2) Novoselov, K. S.; Geim, A. K.; Morozov, S. V.; Jiang, D.; Katsnelson, M. I.; Grigorieva, I. V.; Dubonos, S. V.; Firsov, A. A. *Nature* **2005**, *438*, 197−200.

(3) Booth, T. J.; Blake, P.; Nair, R. R.; Jiang, D.; Hill, E. W.; Bangert, U.; Bleloch, A.; Gass, M.; Novoselov, K. S.; Katsnelson, M. I.; Geim, A. K. *Nano Lett.* **2008**, *8*, 2442−2446.

(4) Pop, E.; Varshney, V.; Roy, A. K. *MRS Bull.* **2012**, *37*, 1273−1281.

(5) Balandin, A. A. *Nat. Mater.* **2011**, *10*, 569−581.

(6) Bonaccorso, F.; Sun, Z.; Hasan, T.; Ferrari, A. C. *Nat. Photonics* **2010**, *4*, 611−622.

(7) Wu, Y.; Lin, Y.; Bol, A. A.; Jenkins, K. A.; Xia, F.; Farmer, D. B.; Zhu, Y.; Avouris, P. *Nature* **2011**, *472*, 74−78.

(8) Chen, C.; Rosenblatt, S.; Bolotin, K. I.; Kalb, W.; Kim, P.; Kymissis, I.; Stormer, H. L.; Heinz, T. F.; Hone, J. *Nat. Nanotechnol.* **2009**, *4*, 861−867.

(9) Merchant, C. A.; Healy, K.; Wanunu, M.; Ray, V.; Peterman, N.; Bartel, J.; Fischbein, M. D.; Venta, K.; Luo, Z.; Johnson, A. T. C.; Drndić, M. *Nano Lett.* **2010**, *10*, 2915−2921.

(10) Venkatesan, B. M.; Estrada, D.; Banerjee, S.; Jin, X.; Dorgan, V. E.; Bae, M. H.; Aluru, N. R.; Pop, E.; Bashir, R. *ACS Nano* **2012**, *6*, 441−450.

(11) Schedin, F.; Geim, A. K.; Morozov, S. V.; Hill, E. W.; Blake, P.; Katsnelson, M. I.; Novoselov, K. S. *Nat. Mater.* **2007**, *6*, 652−655.

(12) Dean, C. R.; Young, A. F.; Meric, I.; Lee, C.; Wang, L.; Sorgenfrei, S.; Watanabe, K.; Taniguchi, T.; Kim, P.; Shepard, K. L.; Hone, J. *Nat. Nanotechnol.* **2010**, *5*, 722−726.

(13) Dorgan, V. E.; Bae, M.-H.; Pop, E. *Appl. Phys. Lett.* **2010**, *97*, 082112-1−082112-3.

(14) Robinson, J. T.; Perkins, F. K.; Snow, E. S.; Wei, Z.; Sheehan, P. E. *Nano Lett.* **2008**, *8*, 3137−3140.

(15) Allen, M. J.; Tung, V. C.; Kaner, R. B. *Chem. Rev.* **2010**, *110*, 132−145.

(16) Kochmann, S.; Hirsch, T.; Wolfbeis, O. S. *TrAC Trends Anal. Chem.* **2012**, *39*, 87−113.

(17) Dan, Y.; Lu, Y.; Kybert, N. J.; Luo, Z.; Johnson, A. T. C. *Nano Lett.* **2009**, *9*, 1472−1475.

(18) Rumyantsev, S.; Liu, G.; Shur, M. S.; Potyrailo, R. A.; Balandin, A. A. *Nano Lett.* **2012**, *12*, 2294−2298.

(19) Salehi-Khojin, A.; Estrada, D.; Lin, K. Y.; Bae, M.-H.; Xiong, F.; Pop, E.; Masel, R. I. *Adv. Mater.* **2012**, *24*, 53−57.

(20) Salehi-Khojin, A.; Estrada, D.; Lin, K. Y.; Ran, K.; Haasch, R. T.; Zuo, J.-M.; Pop, E.; Masel, R. I. *Appl. Phys. Lett.* **2012**, *100*, 033111-1−033111-4.

(21) Fowler, J. D.; Allen, M. J.; Tung, V. C.; Yang, Y.; Kaner, R. B.; Weiller, B. H. *ACS Nano* **2009**, *3*, 301−306.

(22) Pearce, R.; Iakimov, T.; Andersson, M.; Hultman, L.; Spetz, A. L.; Yakimova, R. *Sens. Actuators, B: Chem.* **2011**, *155*, 451−455.

(23) Banhart, F.; Kotakoski, J.; Krasheninnikov, A. V. *ACS Nano* **2011**, *5*, 26−41.

(24) Huang, P. Y.; Ruiz-Vargas, C. S.; Van der Zande, A. M.; Whitney, W. S.; Levendorf, M. P.; Kevek, J. W.; Garg, S.; Alden, J. S.; Hustedt, C. J.; Zhu, Y.; Park, J.; McEuen, P. L.; Muller, D. A. *Nature* **2011**, *469*, 389−392.

(25) Salehi-Khojin, A.; Field, C. R.; Yeom, J.; Masel, R. I. *Appl. Phys. Lett.* **2010**, *96*, 163110-1−163110-3.

(26) Salehi-Khojin, A.; Lin, K. Y.; Field, C. R.; Masel, R. I. *Science* **2010**, *329*, 1327−1330.

(27) Robinson, J. A.; Snow, E. S.; Bădescu, Ş. C.; Reinecke, T. L.; Perkins, F. K. *Nano Lett.* **2006**, *6*, 1747−1751.

(28) Huang, B.; Li, Z.; Liu, Z.; Zhou, G.; Hao, S.; Wu, J.; Gu, B.-L.; Duan, W. *J. Phys. Chem. C* **2008**, *112*, 13442−13446.

(29) Hajati, Y.; Blom, T.; Jafri, S. H. M.; Haldar, S.; Bhandary, S.; Shoushtari, M. Z.; Eriksson, O.; Sanyal, B.; Leifer, K. *Nanotechnology* **2012**, *23*, 505501−505506.

(30) Dresselhaus, M. S.; Jorio, A.; Hofmann, M.; Dresselhaus, G.; Saito, R. *Nano Lett.* **2010**, *10*, 751−758.

(31) Meyer, J. C.; Kisielowski, C.; Erni, R.; Rossell, M. D.; Crommie, M. F.; Zettl, A. *Nano Lett.* **2008**, *8*, 3582−3586.

(32) Buchowicz, G.; Stone, P. R.; Robinson, J. T.; Cress, C. D.; Beeman, J. W.; Dubon, O. D. *Appl. Phys. Lett.* **2011**, *98*, 32102-1−32102-3.

(33) Graf, D.; Molitor, F.; Ensslin, K.; Stampfer, C.; Jungen, A.; Hierold, C.; Wirtz, L. *Nano Lett.* **2007**, *7*, 238−242.

(34) Ryu, S.; Liu, L.; Berciaud, S.; Yu, Y.-J.; Liu, H.; Kim, P.; Flynn, G. W.; Brus, L. E. *Nano Lett.* **2010**, *10*, 4944−4951.

(35) Bae, M. H.; Islam, S.; Dorgan, V. E.; Pop, E. *ACS Nano* **2011**, *5*, 7936−7944.

(36) Lu, G.; Park, S.; Yu, K.; Ruoff, R. S.; Ocola, L. E.; Rosenmann, D.; Chen, J. *ACS Nano* **2011**, *5*, 1154−1164.

(37) Ganji, M. D.; Tajbakhsh, M.; Laffafchy, M. *Solid State Sci.* **2010**, *12*, 1547−1553.

(38) Fagan, S. B.; Souza Filho, A. G.; Lima, J. O. G.; Filho, J. M.; Ferreira, O. P.; Mazali, I. O.; Alves, O. L.; Dresselhaus, M. S. *Nano Lett.* **2004**, *4*, 1285−1288.

(39) Leenaerts, O.; Partoens, B.; Peeters, F. *Phys. Rev. B* **2008**, *77*, 125416−125421.

(40) Fan, X. F.; Zheng, W. T.; Chihaia, V.; Shen, Z. X.; Kuo, J.-L. *J. Phys.: Condens. Matter* **2012**, *24*, 305004−305013.

(41) Romero, H. E.; Shen, N.; Joshi, P.; Gutierrez, H. R.; Tadigadapa, S. A.; Sofo, J. O.; Eklund, P. C. *ACS Nano* **2008**, *2*, 2037−2044.

(42) Wehling, T. O.; Lichtenstein, A. I.; Katsnelson, M. I. *Appl. Phys. Lett.* **2008**, *93*, 202110−202112.

(43) Levesque, P. L.; Sabri, S. S.; Aguirre, C. M.; Guillemette, J.; Siaj, M.; Desjardins, P.; Szkopek, T.; Martel, R. *Nano Lett.* **2011**, *11*, 132−137.

(44) Pinto, H.; Jones, R.; Goss, J. P.; Briddon, P. R. *J. Phys.: Condens. Matter* **2009**, *21*, 402001−402003.

(45) Messina, F.; Cannas, M. *J. Phys. Chem. C* **2007**, *111*, 6663−6667.

(46) Edwards, A. H. *Phys. Rev. B* **1991**, *44*, 1832−1838.